

BUTP-96-30

October 1996

# Prompt $J/\psi$ production at $e^+e^-$ colliders

Feng Yuan

Department of Physics, Peking University, Beijing 100871, People's Republic of China

Cong-Feng Qiao

China Center of Advanced Science and Technology (World Laboratory), Beijing 100080, People's Republic of China

Kuang-Ta Chao

China Center of Advanced Science and Technology (World Laboratory), Beijing 100080, People's Republic of China

Department of Physics, Peking University, Beijing 100871, People's Republic of China

## Abstract

In this paper, we discuss the prompt  $J/\psi$  production at  $e^+e^-$  colliders via color-singlet and color-octet production mechanisms. The color-singlet production processes include 1)  $e^+e^- \rightarrow J/\psi + gg$ ; 2)  $e^+e^- \rightarrow J/\psi + c\bar{c}$ ; 3)  $e^+e^- \rightarrow q\bar{q}ggJ/\psi$  and  $e^+e^- \rightarrow q\bar{q}g_c$  followed by  $g_c \rightarrow J/\psi$ . The color-octet production processes include 1)  $e^+e^- \rightarrow J/\psi + g$ ; 2)  $e^+e^- \rightarrow J/\psi + q\bar{q}$ . Of all these production channels, we find that the color-octet contributions dominate over the color-singlet contributions at any energy scales. At low energies ( $\sqrt{s} < 20\text{ GeV}$ ), the dominant channel is  $e^+e^- \rightarrow J/\psi + g$  whereas at high energies  $e^+e^- \rightarrow J/\psi + q\bar{q}$  will take the leading part. We also find that the energy spectrum for the color-octet  $J/\psi$  production in process  $e^+e^- \rightarrow J/\psi + q\bar{q}$  is very soft, and the mean energy of the produced  $J/\psi$  is only about  $10\text{ GeV} \sim 20\text{ GeV}$  even at very high energies (e.g. at  $1000\text{ GeV}$ ). The extraction of color-octet matrix elements from  $J/\psi$  production in  $e^+e^-$  collisions is also discussed.

PACS number(s): 13.60.Le, 13.20.Gd

## I. INTRODUCTION

Since the first charmonium state  $J/\psi$  was discovered in 1974, the studies of heavy quarkonium states (include charmonium and bottomonium) have played an important role in elementary particle physics. Charmonium and bottomonium are the simplest quark-antiquark composite particles, which can be described by the gauge theory Quantum Chromodynamics (QCD). The investigation of their properties, such as the production and decays may help us to reveal the properties of QCD in both perturbative and nonperturbative sectors. In particular, the  $J/\psi$  production is of special significance because it has extremely clean signature through its leptonic decay modes. Therefore if the heavy quarkonium production mechanism is clarified,  $J/\psi$  triggers can be used as a powerful tool in studying other interesting physics.

The studies of heavy quarkonium production in recent years are mainly stimulated by large discrepancies between the color-singlet model (CSM) predictions and the recent experimental data of CDF at Fermilab Tevatron [1]. There is orders of magnitude disagreement between them. In the color-singlet model description for the quarkonium states, the quark-antiquark pairs are created in colorless configurations. In the past few years, a rigorous framework for treating quarkonium production and decays has been advocated by Bodwin, Braaten and Lepage in the context of nonrelativistic quantum chromodynamics (NRQCD) [2]. In this approach, the production process is factorized into short and long distance parts, while the latter is associated with the nonperturbative matrix elements of four-fermion operators. Another outstanding feature of NRQCD is that it treats the quarkonium not simply as a quark-antiquark pair in color-singlet but rather a superposition of Fock states. Although generally the color-singlet takes a more important role in quarkonium production and decays, the other high Fock states may be dominant in some cases. Under this framework, one can calculate the inclusive production and decay rates to any order in strong coupling constants  $\alpha_s$  as well as  $v^2$ , the relative velocity of heavy quarks inside the bound state. Just with this mechanism, the authors of Ref.[3-5] have successfully explained the  $J/\psi$  ( $^0$ ) and production surplus problems discovered by CDF group.

$J/\psi$  production in  $e^+e^-$  annihilation process has been investigated by several authors within color-singlet model [6-11]. Recently, Braaten and Chen have noted that a clean signature of color-octet mechanism may be observed in the angular distribution of  $J/\psi$  production

near the endpoint region at  $e^+e^-$  collider [12]. In this paper, we make a thorough discussion about the  $J=$  production at  $e^+e^-$  colliders, including color-singlet and color-octet contributions. The rest of the paper is organized as follows. In Sec.II, we discuss the  $J=$  production color-singlet processes, including 1)  $e^+e^- \rightarrow J=gg$ ; 2)  $e^+e^- \rightarrow J=\alpha\alpha$ ; 3)  $e^+e^- \rightarrow q\bar{q}ggJ=$  and  $e^+e^- \rightarrow q\bar{q}g_c$  followed by  $g_c \rightarrow J=$ . We carefully study the characters of each channel. In Sec.III, we study the color-octet production mechanism, including 1)  $e^+e^- \rightarrow J=g$ ; 2)  $e^+e^- \rightarrow J=q\bar{q}$ . Comparisons of the energy scaling properties as well as energy spectrum of these processes are made. In Sec.IV, we give a short discussion about the determination of color-octet matrix elements, and find that they can be extracted from  $e^+e^-$  collision experiments at different energy regions. Finally, we briefly discuss our results and make a conclusion in Sec.V.

## II. COLOR-SINGLET CONTRIBUTIONS

The leading order color-singlet contributions to direct  $J=$  production include the following processes

$$e^+e^- \rightarrow \alpha\alpha \quad J=\alpha\alpha; \quad (1)$$

$$e^+e^- \rightarrow gg \quad J=gg; \quad (2)$$

$$e^+e^- \rightarrow q\bar{q}g \quad \text{with } g \rightarrow J=gg; \quad (3)$$

The relevant Feynman diagrams are shown in Fig.1. Fig.1 (a) is a quark process, Fig.1 (b) is a gluon process, Fig.1 (c) and Fig.1 (d) are gluon jets processes. All these three processes have been calculated separately in literatures [8-11]. Here, we make a comparison of the relative weight of them as a function of c.m. energy  $\sqrt{s}$ .

For the quark process, the calculation is straightforward, and we get [11]

$$\frac{d\sigma(e^+e^- \rightarrow J=\alpha\alpha)}{dzdx_1} = \frac{32}{243} \frac{e_c^2 \langle O_1(^3S_1) \rangle}{m^3} \frac{\sum_{i=1}^4 F_i r^i}{(1-x_1)^2 (2-z)^2 (z+x_1-1)^4}; \quad (4)$$

where

$$z = \frac{2p}{s} \frac{k}{s}; \quad x_1 = \frac{2p_1}{s} \frac{k}{s}; \quad r = \frac{m^2}{s}; \quad (5)$$

$$= \sigma_{\text{QED}} (e^+ e^- \rightarrow J^+ J^-):$$

$k$ ,  $p$  and  $p_1$  are the momenta of virtual photon,  $J^0$ , and outgoing parton (c quark in Fig.1 (a), gluon in Fig.1 (b)), respectively;  $m$  is the mass of  $J^0$ , which equals to  $2m_c$  at nonrelativistic approximation;  $\langle O_1(^3S_1) \rangle$  is the color-singlet nonperturbative matrix element; The functions  $F_i$  are defined as

$$F_1 = 2(x_1 + z - 1)^2 (x_1 - 1) [4x_1^3 - 6x_1^2 (z^2 - 2z + 2) - 2x_1 (4z^3 - 15z^2 + 12z - 2) - 11z^4 + 23z^3 - 24z^2 + 8z + 4];$$

$$F_2 = (x_1 + z - 1) [16x_1^5 + 4x_1^4 (5z - 4) + 4x_1^3 (3z^2 - 4z - 24) + \frac{2}{3} (5z^3 + 16z^2 - 180z + 256) + x_1 (7z^4 + 30z^3 - 132z^2 + 360z - 256) + 11z^4 - 55z^3 + 136z^2 - 200z + 96];$$

$$F_3 = 8(4x_1^5 - 14x_1^4 + 31x_1^3 - 50x_1^2 + 43x_1 - 14) + 4z(14x_1^4 - 62x_1^3 + 149x_1^2 - 184x_1 + 83) + 2z^2(21x_1^3 - 130x_1^2 + 269x_1 - 176) + z^3(29x_1^2 - 154x_1 + 177) + 4z^4(4x_1 - 11) + 5z^5;$$

$$F_4 = 3(4x_1^3 + 4x_1^2 z - 4x_1^2 - 4x_1 - z^3 + 4z^2 - 8z + 4)(2x_1 + z - 2); \quad (6)$$

After integrating Eq.(4) over  $x_1$ , and considering the fragmentation approximation (i.e.,  $\frac{p}{s} \rightarrow m_c, r \rightarrow 1$ ), the differential cross section reads as

$$\frac{d}{dz} (e^+ e^- \rightarrow J^0 \gamma) = 2 (e^+ e^- \rightarrow \gamma \gamma) D_{c|J^0}(z); \quad (7)$$

where  $D_{c|J^0}(z)$  denotes the quark fragmentation function. Its explicit form may be found in Ref. [13].

As for the gluon process Fig.1 (b), from Ref. [8] we readily have

$$\frac{d(e^+ e^- \rightarrow J^0 gg)}{dz dx_1} = \frac{64e_c^2}{81} \frac{\langle O_1(^3S_1) \rangle}{m^3} r^2 f(z; x_1; r); \quad (8)$$

where

$$f(z; x_1; r) = \frac{(2 + x_2)x_2}{(2 - z)^2 (1 - x_1 - r)^2} + \frac{(2 + x_1)x_1}{(2 - z)^2 (1 - x_2 - r)^2} + \frac{(z - r)^2 - 1}{(1 - x_2 - r)^2 (1 - x_1 - r)^2} + \frac{1}{(2 - z)^2 (1 - x_2 - r)^2 (1 - x_1 - r)^2} \frac{6(1 + r - z)^2}{(1 - x_2 - r)(1 - x_1 - r)r} + \frac{1}{r}; \quad (9)$$

the variables  $z; x_1; r$  are defined as Eq.(5) and  $x_2 = 2 - z - x_1$ .

$J = \text{production from gluon jets processes as shown in Fig.1 (c) and Fig.1 (d) have been calculated in Ref. [10], giving}$

$$\langle e^+ e^- \rightarrow q\bar{q}g; g \rightarrow J = X \rangle = \frac{Z^S}{m^2} \langle e^+ e^- \rightarrow q\bar{q}g \rangle P(g \rightarrow J = X); \quad (10)$$

where  $\square = m^2(g)$  is the virtuality of the gluon.  $P(g \rightarrow J = X)$  is the decay distribution function of virtual gluon to  $J = \text{, which includes the contributions directly from } g \rightarrow J = g\bar{g}$  and from E1 transitions of  $\psi_c(g) \rightarrow g \psi_c$  followed by  $\psi_c \rightarrow J = \text{. We can express it as}$

$$P(g \rightarrow J = X) = P_S(g \rightarrow J = g\bar{g}) + Br(\psi_c \rightarrow J = \text{) } P(g \rightarrow \psi_c g); \quad (11)$$

where

$$P_S(g \rightarrow J = g\bar{g}) = \frac{10}{243} \frac{\langle O_1(^3S_1) \rangle}{m^3} \frac{r^2}{2} \int_{z^P \bar{r}}^{z^+ r} dz dx_1 f(z; x_1; r); \quad (12)$$

Here the function  $f(z; x_1; r)$  is defined as Eq.(9) with  $r = m^2 = \text{. The integration limits of } x_1 \text{ are}$

$$x_1 = \frac{1}{2} (2 - z - \frac{P}{z^2 - 4r}); \quad (13)$$

Because the  $g \rightarrow \psi_c g$  processes have the infrared divergence involved, which are associated with the soft gluon in the final states, we induce an infrared cutoff to avoid the singularities in  $P(g \rightarrow \psi_c g)$ . Strictly speaking, the divergences can be cancelled in the framework of NRQCD (see Ref. [14]). Here, we follow the way of Ref. [15] by imposing a lower cutoff on the energy of the outgoing gluon in the quarkonium rest frame. Then, the decay distribution functions for  $\psi_c$  can be written as

$$P(g \rightarrow \psi_c g) = \frac{8}{9} \frac{\mathcal{R}_P^0(0)^2}{m^5} \frac{r(1 - 3r^2)}{1 - r} \left( \frac{1}{r} - \frac{1}{m_c} - 1 \right); \quad (14)$$

$$P(g \rightarrow \psi_{c1} g) = \frac{8}{9} \frac{\mathcal{R}_P^0(0)^2}{m^5} \frac{6r(1 + r)}{1 - r} \left( \frac{1}{r} - \frac{1}{m_c} - 1 \right); \quad (15)$$

$$P(g \rightarrow \psi_{c2} g) = \frac{8}{9} \frac{\mathcal{R}_P^0(0)^2}{m^5} \frac{2r(1 + r + 6r^2)}{1 - r} \left( \frac{1}{r} - \frac{1}{m_c} - 1 \right); \quad (16)$$

As discussed in Ref. [15], the cutoff can be set to  $m_c$  in order to avoid the large logarithms in the divergent terms.

With the above formulas, we can evaluate the prompt  $J=$  production rates of color-singlet processes in  $e^+e^-$  annihilation at any energy regions. The results are displayed in Fig 2 and Fig 3, the input parameters used in the numerical calculations are [16] [17]

$$m_u = m_d = m_s = 0; \quad m_c = 1.5 \text{ GeV}; \quad m_b = 4.9 \text{ GeV}; \quad \alpha_s(2m_c) = 0.26; \quad (17)$$

$$\langle O_1(^3S_1) \rangle = 0.73 \text{ GeV}^3; \quad \mathcal{R}_P^0(0) f = 0.125 \text{ GeV}^5; \quad (18)$$

The branching ratios of  $\psi \rightarrow J=$  taking in the calculations are [18]

$$\begin{aligned} \text{Br}(\psi \rightarrow J=) &= 6.6 \times 10^{-3}; \\ \text{Br}(\psi \rightarrow J=) &= 27.3\%; \\ \text{Br}(\psi \rightarrow J=) &= 13.5\%; \end{aligned} \quad (19)$$

The angular distribution and energy distribution of color-singlet  $J=$  production at CLEO have been discussed in Ref. [11]. Here, we make a comparison of the relative importance of these three color-singlet processes as a function of c.m. energy  $\sqrt{s}$ . The result is displayed in Fig 2. The dotted line demonstrates the contribution from quark process (1), the dash line is from gluon process (2), the dotted-dash line is from gluon jets processes (3), and the solid line is the total color-singlet cross section. From this figure, we can see that at low energies ( $\sqrt{s} = 25 \text{ GeV}$ ) the gluon process dominates the other two processes, at somewhat high energies the quark process will dominate, and at high enough energies, the gluon jets processes are dominant. To see the sensitivity of quark fragmentation approximation to interaction energy  $\sqrt{s}$ , we also plot the line corresponding to the quark fragmentation approximation Eq.(7) in the same figure. Obviously, the quark process at high energies can be represented by the quark fragmentation approximation. The diagrams show that at  $\sqrt{s} = 70 \text{ GeV}$  the difference between the complete calculation and the fragmentation approximation is less than 5%. Another striking result is that the process (3) is negligible at low energies, but at high enough energies ( $\sqrt{s} = 200 \text{ GeV}$ ) its contribution dominates the other two processes and grows with the energy increases.

In Fig 3, We display the energy distributions of quark process, gluon process, and their sum at  $\sqrt{s}$  to be 10.6 GeV, 25 GeV, 50 GeV and 100 GeV respectively. At low energies, such as at CLEO ( $\sqrt{s} = 10.6 \text{ GeV}$ ), the energy spectrum of these two processes are both at

(see Fig.3 (a)), however, at high energies the patterns of the energy spectrum of these two processes are distinct. The quark process is hard and the gluon process is soft (see Fig.3 (c)-(d)). After the relative importance of these two processes is changed with c.m. energy, the energy distribution feature of the total cross section of these two processes is also changed with c.m. energy. Therefore, at high enough energies, the distribution is mainly from quark process, and the total spectrum appears hard (see Fig.3 (a)-(d)).

### III. COLOR-OCTET CONTRIBUTIONS

The leading order color-octet contributions to direct  $J/\psi$  production in  $e^+e^-$  collision include the following two processes

$$\text{i) } e^+e^- \rightarrow \psi + q\bar{q} + \mathcal{O}(\alpha_s^3 S_1); \quad (20)$$

$$\text{ii) } e^+e^- \rightarrow \psi + g + \mathcal{O}(\alpha_s^{2S+1} L_J); \quad (21)$$

as shown in Fig.4. Here  $^{2S+1}L_J$  denotes the states  $^1S_0$  and  $^3P_J$ ,  $q$  represents the  $u; d; s; c$  and  $b$  quarks.

As the first process shown in Fig.4 (a), using the factorization formalism described in Ref. [2], we can write the differential cross section as

$$d(e^+e^- \rightarrow \psi + q\bar{q}) = d^{\wedge}(e^+e^- \rightarrow q\bar{q}) \mathcal{O}_8(^3S_1) < \mathcal{O}_8(^3S_1) >; \quad (22)$$

where  $d^{\wedge}$  represents the short distance coefficient of the process, which can be calculated perturbatively.  $< \mathcal{O}_8(^3S_1) >$  corresponds to the long distance nonperturbative matrix element. It can be treated as free parameter or evaluated by fitting the theory to experimental data. The result is

$$\frac{d(e^+e^- \rightarrow \psi + q\bar{q})}{ds_1 ds_2} = \frac{e_q^2 s^2}{12} \frac{< \mathcal{O}_8(^3S_1) >}{m_c^3} \frac{\sum_{i=0}^{P^3} G_i s_2^i}{s^2 (s_1 - m_q^2) (s_2 - m_q^2) (s - m^2 - m_q^2)}; \quad (23)$$

where

$$s_1 = (k - p)^2; \quad s_2 = (k - p_1)^2;$$

In the above,  $k$  is the momentum of virtual photon,  $p$  and  $p_1$  are the momenta of outgoing  $J/\psi$  and quark  $q$ ,  $m_q$  is the mass of the quark and  $e_q$  is its charge. The integration limits of  $s_1$  and  $s_2$  are

$$s_1 = m^2 + m_q^2 - \frac{1}{2s_2} [s_2 (s_2 - s + m^2) - \frac{1}{2} (s_2; s; m^2) - \frac{1}{2} (s_2; m_q^2; m_q^2)]; \quad (24)$$

$$s_2 = 4m_q^2; \quad s_2^+ = (P - m)^2; \quad (25)$$

is defined as

$$(x; y; z) = x^2 + y^2 + z^2 - 2xy - 2yz - 2xz;$$

The functions  $G_i$  are

$$\begin{aligned} G_0 &= 3m^6 m_q^2 + 4m^2 m_q^6 + 7m^4 m_q^4 + 2m_q^8 + s(m^6 + 4m_q^6 + m^6 + 11m^4 m_q^2 + 16m^2 m_q^4) \\ &\quad + s^2(2m^4 + 11m^2 m_q^2 + 7m_q^4) + s^3(m^2 + 3m_q^2) + s_1(m^6 - 6m^4 m_q^2 - 5m^4 s \\ &\quad - 12m^2 m_q^4 - 16m^2 m_q^2 s - 5m^2 s^2 - 8m_q^6 - 12m_q^4 s - 6m_q^2 s^2 - s^3) + s_1^2(3m^4 \\ &\quad + 12m^2 m_q^2 + 8m^2 s + 12m_q^4 + 12m_q^2 s + 3s^2) + 4s_1^3(m^2 - 2m_q^2 - s) + 2s_1^4; \\ G_1 &= -5m^4 m_q^2 - 8m^2 m_q^4 - 2s(m^4 + 6m^2 m_q^2 + 4m_q^4) - s^2(2m^2 + 5m_q^2) \\ &\quad + s_1(m^4 + 4m^2 m_q^2 + 4m_q^4 + 4s(m^2 + m_q^2) + s^2) + 4s_1^2(m^2 - 2m_q^2 - s) + 4s_1^3; \\ G_2 &= 3m^2 m_q^2 + m^2 s - m^2 s_1 + 3m_q^4 + 3m_q^2 s - 2m_q^2 s_1 - s s_1 + 3s_1^2; \\ G_3 &= s_1 - m_q^2; \end{aligned} \quad (26)$$

A check can be performed by considering the high energy limit in this process. At high enough energies, the outgoing quark mass  $m_q$  can be neglected. Setting  $m_q = 0$ , and integrating over  $s_1$  and  $s_2$ , we will obtain

$$\begin{aligned} \frac{(\epsilon^+ \epsilon^- \rightarrow J = qq)}{96} &= \frac{e_q^2 s^2 (2m_c) \langle O_8(^3S_1) \rangle}{m^3} f_5(1-r^2) - 2r \ln r \\ &\quad + [2Li_2\left(\frac{r}{1+r}\right) - 2Li_2\left(\frac{1}{1+r}\right) \\ &\quad - 2 \ln(1+r) \ln r + 3 \ln r + \ln^2 r](1+r)^2 g; \end{aligned} \quad (27)$$

where  $Li_2(x) = \int_0^x \frac{dt}{t} \ln(1-t)$  is the Spence function. The result here is completely consistent with that in Ref. [19], in which the charmonium production in  $Z^0$  decays through the similar process is calculated.

The second process as shown in Fig.4 (b) has been calculated in Ref. [12], giving

$$(\epsilon^+ \epsilon^- \rightarrow J = g) = C_s \langle O_8(^1S_0) \rangle + C_p \langle O_8(^3P_0) \rangle; \quad (28)$$

$$C_s = \frac{64 e_c^2 s^2}{3} \frac{1-r}{s^2 m}; \quad (29)$$

$$C_p = \frac{256 e_c^2 s^2}{9s^2 m^3} \left[ \frac{(1-3r)^2}{1-r} + \frac{6(1+r)}{1-r} + \frac{2(1+3r+6r^2)}{1-r} \right]; \quad (30)$$



where we have used the approximate heavy quark spin symmetry relations:

$$\langle O_8(^3P_J) \rangle = (2J + 1) \langle O_8(^3P_0) \rangle : \quad (31)$$

Up to now, the color-octet matrix elements  $\langle O_8(^3S_1) \rangle$ ,  $\langle O_8(^1S_0) \rangle$  and  $\langle O_8(^3P_0) \rangle$  are determined only by fitting to the experimental data.  $\langle O_8(^3S_1) \rangle$  is extracted from hadroproduction process at the Tevatron [2][3] [16]. The results are consistent with the theoretical anticipation of NRQCD. As for  $\langle O_8(^1S_0) \rangle$  and  $\langle O_8(^3P_0) \rangle$ , they have been obtained from both hadroproduction and photoproduction, but the results from different processes are incompatible (see Ref. [20]), which we will give a detailed discussion in Sec.IV. Here, we tentatively choose the color-octet matrix elements obtained in Ref. [4] [16], which are consistent with the velocity scaling rules,

$$\langle O_8(^3S_1) \rangle = 1.5 \times 10^{-2} \text{GeV}^3; \quad (32)$$

$$\langle O_8(^1S_0) \rangle = 10^{-2} \text{GeV}^3; \quad (33)$$

$$\frac{\langle O_8(^3P_0) \rangle}{m_c^2} = 10^{-2} \text{GeV}^3; \quad (34)$$

Using the input parameters as in Sec.II, we can calculate the intermediate color-octet contributions to  $J/\psi$  production in  $e^+e^-$  collisions. From Eq.(23)–(26) and Eq.(28)–(34), the contributions of these two processes to  $J/\psi$  production rates as a function of c.m. energy  $\sqrt{s}$  may be obtained as shown in Fig.5. The dotted line is from process (ii), the dotted-dash line is from process (i), the solid line is the sum of them, and the dash line is the total cross section of color-singlet processes contributions. From this diagram, we can see that at low energies the dominant process is channel (ii), at higher energies ( $\sqrt{s} > 20 \text{GeV}$ ) the channel (i) dominates. It is interesting to note that the color-octet contributions dominate the color-singlet contributions at any energy values of  $\sqrt{s}$ . So if the color-octet production mechanism is correct and the color-octet matrix elements are not far smaller with values used here,  $J/\psi$  production in  $e^+e^-$  collision mainly comes from color-octet contributions.

Another important character of the color-octet  $J/\psi$  production in  $e^+e^-$  collision is its energy spectrum. The energy spectrum of process (ii) has been discussed in Ref. [12]. In this process,  $J/\psi$ 's energy mainly lies at the endpoint region which equals half of the c.m. energy, its width is about  $(\frac{2m_c}{\sqrt{s}} \approx 500) \text{MeV}$ . In contrast, the energy spectrum of process (i) is very soft. As shown in Fig.6, the energy distribution of  $J/\psi$  production in process

(i) is mainly from low energy region even at high cm . energies ( 500G eV ). Numerical result shows, the mean energy value of  $J=\text{from process (i)}$  is about 10G eV 20G eV at any energy value of  $P_{\text{S}}$  less than 1000G eV .

#### IV . C O L O R - O C T E T M A T R I X E L E M E N T S

Unlike color-singlet matrix elements which associate with the quarkonium radial wave function at the origin in the nonrelativistic limit, and can be calculated by potential model [17], the color-octet matrix elements are unknown. They can be extracted from experimental data or from lattice QCD calculations. Before lattice QCD giving out the results, the color-octet matrix elements are determined only by fitting the theoretical prediction to experimental data. As done in the literatures [2-4] [16] [20] [21], the color-octet matrix elements are extracted from experimental data of  $J=\text{production}$  in hadron collisions and  $e^+e^-$  collisions. In these processes, the production mechanism is associated with the structure function of hadrons, therefore there are still left a lot of uncertainties, e.g. the higher twist effects, which we can not handle clearly now . Therefore, the extraction of octet matrix elements from these different processes certainly exists large theoretical uncertainties, even their results are not consistent with each other [20] [21]. In contrast, the mechanism of  $J=\text{production}$  in  $e^+e^-$  annihilation process is much clearer than those hadron processes discussed above. The parton structure is simpler, and there is no higher twist effects to be considered, so the theoretical uncertainty is much smaller. Following, we discuss the possibility of extracting elements  $\langle O_8(^3S_1) \rangle$  ,  $\langle O_8(^1S_0) \rangle$  and  $\langle O_8(^1S_0) \rangle$  from  $e^+e^-$  annihilation experiments.

>From the results of Sec.III, the color-octet contributions dominate the color-singlet contributions at any energy regions. The total cross section of  $J=\text{production}$  in  $e^+e^-$  collision is sensitive to the color-octet matrix elements. So, we can precisely extract them from fitting the theoretical prediction to the experimental data. Furthermore, there is another important feature of color-octet  $J=\text{production}$  in  $e^+e^-$  process, that the relative importance of these octet processes are distinct at different energy regions. At high energies, the element  $\langle O_8(^3S_1) \rangle$  is important, while at low energies,  $\langle O_8(^1S_0) \rangle$  and  $\langle O_8(^3P_0) \rangle$  are important. So, we can extract them separately from different energy experiments.

$\langle \sigma_8(^1S_0) \rangle$  was determined previously from hadroproduction at the Fermilab Tevatron. In Ref. [16], the authors use the gluon fragmentation approximation at high  $P_T$  to fit the experimental data. They obtain

$$\langle \sigma_8(^3S_1) \rangle = 1.5 \cdot 10^{-2} \text{ GeV}^3: \quad (35)$$

In Ref. [4], the authors extend out the gluon fragmentation region, and take a global fitting to the experimental data (at  $P_T > 5 \text{ GeV}$ ) including  $\langle \sigma_8(^3S_1) \rangle$ ,  $\langle \sigma_8(^1S_0) \rangle$  and  $\langle \sigma_8(^3P_0) \rangle$  contributions, get

$$\langle \sigma_8(^3S_1) \rangle = 6.6 \cdot 10^{-3} \text{ GeV}^3: \quad (36)$$

At LEP II energy region ( $\sqrt{s} = 160 \text{ GeV}$ ), the color-octet production cross section  $\sigma_8$  is about 6 times larger than the color-singlet process cross section  $\sigma_1$ , and the former mainly comes from the contribution of  $\langle \sigma_8(^3S_1) \rangle$  (the contributions from  $\langle \sigma_8(^1S_0) \rangle$  and  $\langle \sigma_8(^3P_0) \rangle$  are small enough and may be neglected, see Fig.5). So,  $\langle \sigma_8(^3S_1) \rangle$  can be extracted by precisely measuring the total cross section of  $J=0$  production in  $e^+e^-$  annihilation at this energy region.

As for the elements  $\langle \sigma_8(^1S_0) \rangle$  and  $\langle \sigma_8(^3P_0) \rangle$ , the situation is more complicated. In previous studies, the values of them were extracted from the experimental data of hadroproduction at high  $P_T$ , photoproduction at forward direction and fixed-target hadroproduction. In Ref. [4], a global fitting to all  $P_T$  region data shows that at low  $P_T$  boundary the theoretical prediction is dominated by the contributions from  $\langle \sigma_8(^1S_0) \rangle$  and  $\langle \sigma_8(^3P_0) \rangle$ , and the fitted result is

$$\langle \sigma_8(^1S_0) \rangle + \frac{3}{m_c^2} \langle \sigma_8(^3P_0) \rangle = 6.6 \cdot 10^{-2}: \quad (37)$$

However, the studies of photoproduction at  $e p$  collisions show that the matrix element values in above equation may be overestimated [20], and the authors obtain another linear combination of these two elements

$$\langle \sigma_8(^1S_0) \rangle + \frac{7}{m_c^2} \langle \sigma_8(^3P_0) \rangle = 2.0 \cdot 10^{-2}: \quad (38)$$

Eqs.(37) and (38) are incompatible. Furthermore, the fixed-target result [21] gives the same argument for the matrix elements values in Eq.(37), and gives

$$\langle O_8(^1S_0) \rangle + \frac{7}{m_c^2} \langle O_8(^3P_0) \rangle = 3.0 \times 10^{-2}; \quad (39)$$

This problem may be further clarified in  $J/\psi$  production in  $e^+e^-$  collision experiment. Because at low energies the  $J/\psi$  production dominantly comes from the color-octet  $^1S_0$  and  $^3P_J$  subprocesses (see Fig.5), and where the associated color-octet matrix elements are  $\langle O_8(^1S_0) \rangle$  and  $\langle O_8(^3P_0) \rangle$ . We can extract another linear combination of these two elements by fitting to the experimental data at this energy regions. Furthermore, the coefficients in front of these two elements in the combination are different at different cm. energy, because the relative importance of these two subprocesses is changed with energy. So we can extract different combinations from different energy experiments. Here we choose two typical cm. energy values,  $\sqrt{s} = 4.6 \text{ GeV}$  (at BEPC) and  $10.6 \text{ GeV}$  (at CLEO), to see what combination of the two elements can be extracted from the experiment. At  $\sqrt{s} = 4.6 \text{ GeV}$ , from Eq.(28) we get

$$a_8 = 0.065 \langle O_8(^1S_0) \rangle + \frac{\langle O_8(^3P_0) \rangle}{m_c^2}; \quad (40)$$

and at  $\sqrt{s} = 10.6 \text{ GeV}$ , the combination is

$$a_8 = 0.26 \langle O_8(^1S_0) \rangle + \frac{\langle O_8(^3P_0) \rangle}{m_c^2}; \quad (41)$$

From these two equations, the individual value of these two elements may be extracted.

## V. CONCLUSIONS

In this paper, we have calculated the direct  $J/\psi$  production in  $e^+e^-$  annihilation including color-singlet and color-octet contributions. We have studied the energy scaling properties as well as energy spectrum of all the production processes. The numerical result shows that the color-octet contributions dominate the color-singlet contributions at any cm. energy scales and the energy spectrum of these two color-octet processes are distinct. That enables us to further carefully study the properties of color-octet  $J/\psi$  production in  $e^+e^-$  collision experiment such as the angular distributions et al..

In this paper, we have concentrated on the  $J/\psi$  production only through the virtual photon in  $e^+e^-$  collisions. The contributions from the  $Z^0$  boson at high energies should be included and will be considered elsewhere.

Because in  $e^+e^-$  processes  $J=$  production has much smaller theoretical uncertainty THAN IN HADRONIC  $J=$  PRODUCTION PROCESSES, it can be used to extract the color-octet matrix elements precisely. At high energies color-octet  $^3S_1$  subprocess is dominant and the element  $\langle O_8(^3S_1) \rangle$  can be extracted from experimental data in this energy region. At low energies color-octet  $^1S_0$  and  $^3P_J$  subprocesses will dominate, one can extract two sets of linear combinations of the elements  $\langle O_8(^1S_0) \rangle$  and  $\langle O_8(^3P_0) \rangle$  from different energy experiments, e.g. at BEPC and CLEO energy regions. From these two combination equations, the individual values of the matrix elements can be obtained separately. This really provides a strong motivation in experiment to extract the color-octet matrix elements in  $e^+e^-$  colliders at now reaching energy. In conclusion, in  $e^+e^-$  annihilation experiment,  $J=$  production signature provides an another criterion in testing the color-octet signals and the NRQCD scaling rules.

## Acknowledgements

One of us (F.Yuan) thanks the staff of the Physics Department Computer Center (Room 540) for their kind help. This work was supported in part by the National Natural Science Foundation of China, the State Education Commission of China and the State Commission of Science and Technology of China.

- 
- [1] CDF collaboration, F.Abe et al, Phys.Rev.Lett. 69, 3704 (1992); Phys.Rev.Lett. 71, 2537 (1993).
  - [2] G.T.Bodwin, E.Braaten and G.P.Lepage, Phys.Rev.D 51, 1125 (1995).
  - [3] E.Braaten and S.Fleming, Phys.Rev.Lett. 74, 3327 (1995); M.Cacciari, M.Greco, M.L.Mangano and A.Petrelli, Phys.Lett.B 356 553 (1995).
  - [4] P.Cho and K.Leibovich, Phys.Rev.D 53, 150 (1996); *ibid*, D 53, 6203 (1996).
  - [5] for a recent review see E.Braaten, S.Fleming, and T.C.Yuan, Report No.hep-ph/9602374 (unpublished).
  - [6] C.H.Chang, Nucl.Phys.B 172 425 (1980); E.L.Berger and D.Jones, Phys.Rev.D 23 1521 (1981); J.H.Kuhn, J.Kaplan and E.G.O.Sani, Nucl.Phys.B 157 125 (1979); B.Guberina, J.H.Kuhn, R.D.Peccei and R.Ruckl, Nucl.Phys.B 174 317 (1980); R.Baier and R.Ruckl, Z.Phys.C 19 251 (1983).

- [7] J.H. Kuhn and H. Schneider, Phys. Rev. D 24 2996 (1981); J.H. Kuhn and H. Schneider, Z. Phys. C 11 253 (1981).
- [8] W. Y. Keung, Phys. Rev. D 23 2072 (1981).
- [9] V.M. Driesen, J.H. Kuhn and E.M. Mirkes, Phys. Rev. D 49 3197 (1994).
- [10] K. Hagiwara, A.D. Martin, and W. J. Stirling, Phys. Lett. B 267, 527 (1991).
- [11] P. Cho and K. Leibovich, Report No. hep-ph/9606229 (unpublished).
- [12] E. Braaten and Y.-Q. Chen, Phys. Rev. Lett. 76 730 (1996).
- [13] E. Braaten, K. Cheung and T.C. Yuan, Phys. Rev. D 48 4230 (1993).
- [14] J.P. Ma, Phys. Lett. B 332, 398 (1994); Nucl. Phys. B 447, 405 (1995).
- [15] E. Braaten and T.C. Yuan, Phys. Rev. D 50, 3176 (1994).
- [16] E. Braaten and T.C. Yuan, Phys. Rev. D 52 6627 (1995).
- [17] E. J. Eichten and C. Quigg, Phys. Rev. D 52, 1726 (1995).
- [18] Particle Data Group, Phys. Rev. D 54, 1 (1996).
- [19] K. Cheung, W. Y. Keung, and T.C. Yuan, Phys. Rev. Lett. 76, 877 (1996).
- [20] M. Cacciari and M. Kramer, Phys. Rev. Lett. 76, 4128 (1996); J. Amundson, S. Fleming, and I. Maksymyk, Report No. hep-ph/9601298; P. Ko, J. Lee, and H. S. Song, Report No. hep-ph/9602223.
- [21] M. Beneke and I.Z. Rothstein, Phys. Rev. D 54 2005 (1996); I.Z. Rothstein, Report No. hep-ph/9609281.

## Figure Captions

Fig.1. Feynman diagrams for direct  $J = \text{color-singlet}$  production processes in  $e^+e^-$  annihilation. (a) quark process  $e^+e^- \rightarrow J = q\bar{q}$ ; (b) gluon process  $e^+e^- \rightarrow J = g\bar{g}$ ; (c) gluon jets process  $e^+e^- \rightarrow q\bar{q}g$  with  $g \rightarrow J = g\bar{g}$ ; (d)  $c$  production from gluon jets in  $e^+e^- \rightarrow q\bar{q}g$  with  $g \rightarrow c\bar{c}$ .

Fig.2. Color-singlet cross section vs c.m. energy. Dotted line illustrates the quark process, dash line shows the gluon process, dotted-dash line comes from gluon jets, and the sum of the three processes is plotted as solid line. The quark fragmentation approximation is also shown as short-dashed curve.

Fig.3. Color-singlet energy distribution  $d\sigma/dz$  as function of  $z$  at different c.m. energy. The distributions from quark process (dotted line), gluon process (dashed line) along with the sum of them (solid line) at (a)  $\sqrt{s} = 10.6 \text{ GeV}$ ; (b)  $\sqrt{s} = 25 \text{ GeV}$ ; (c)  $\sqrt{s} = 50 \text{ GeV}$ ; (d)  $\sqrt{s} = 100 \text{ GeV}$ .

Fig.4. Feynman diagrams for direct  $J = \text{color-octet}$  production processes in  $e^+e^-$  annihilation. (a)  $e^+e^- \rightarrow q\bar{q}J = \text{color-octet}$ ; (b)  $e^+e^- \rightarrow J = g$ .

Fig.5. Color-octet cross section vs c.m. energy. Process (i) contribution is represented as the dotted-dash line, process (ii) as the dotted line, and the sum as the solid line. The color-singlet contribution is drawn as dashed line.

Fig.6. Energy spectrum of produced  $J = \text{color-octet}$  process (i) at different c.m. energies. From up to down, the curves represent  $\sqrt{s} = 1000 \text{ GeV}$ ,  $500 \text{ GeV}$ ,  $200 \text{ GeV}$ ,  $100 \text{ GeV}$ , and  $50 \text{ GeV}$  respectively.

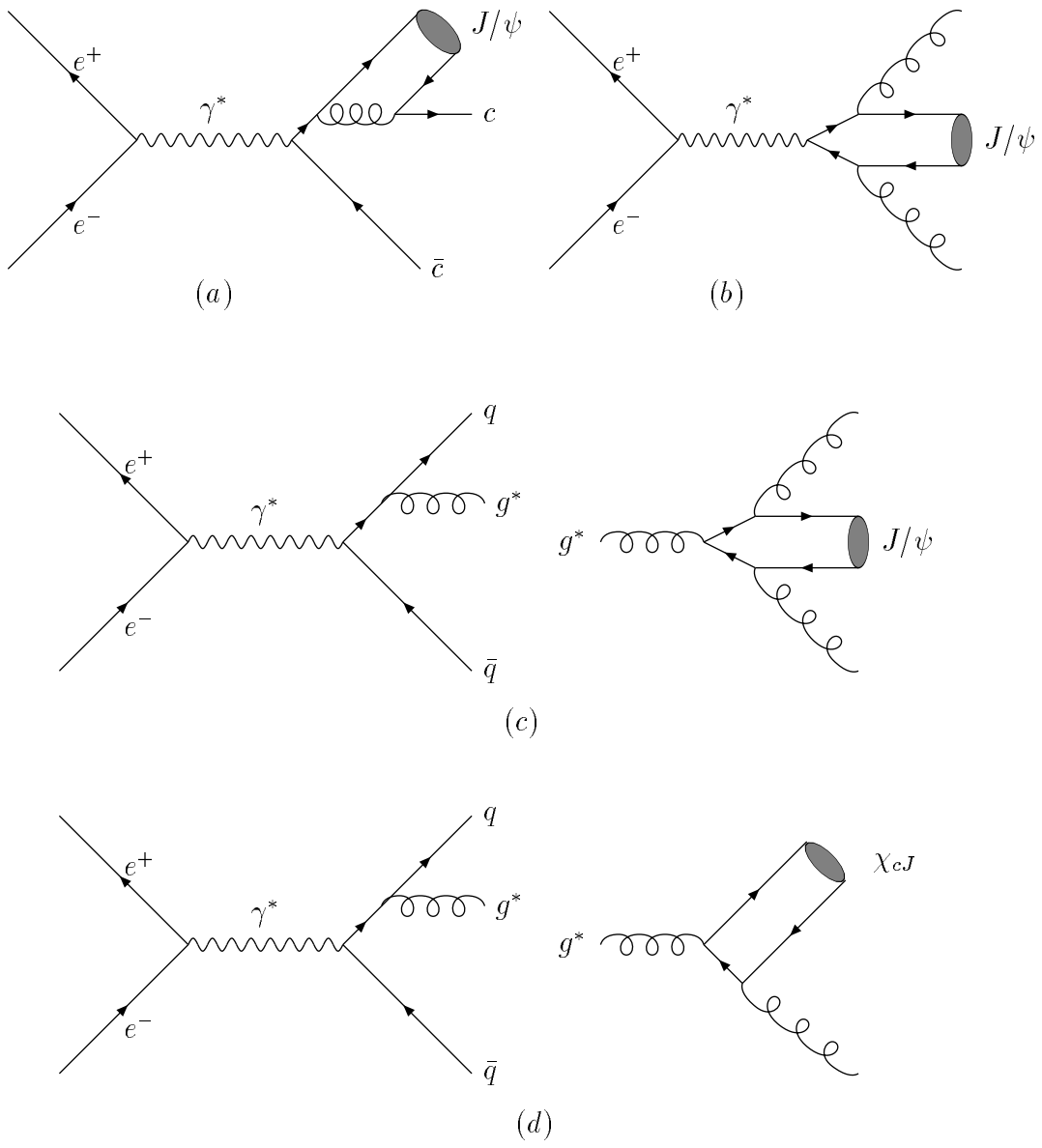


Fig.1



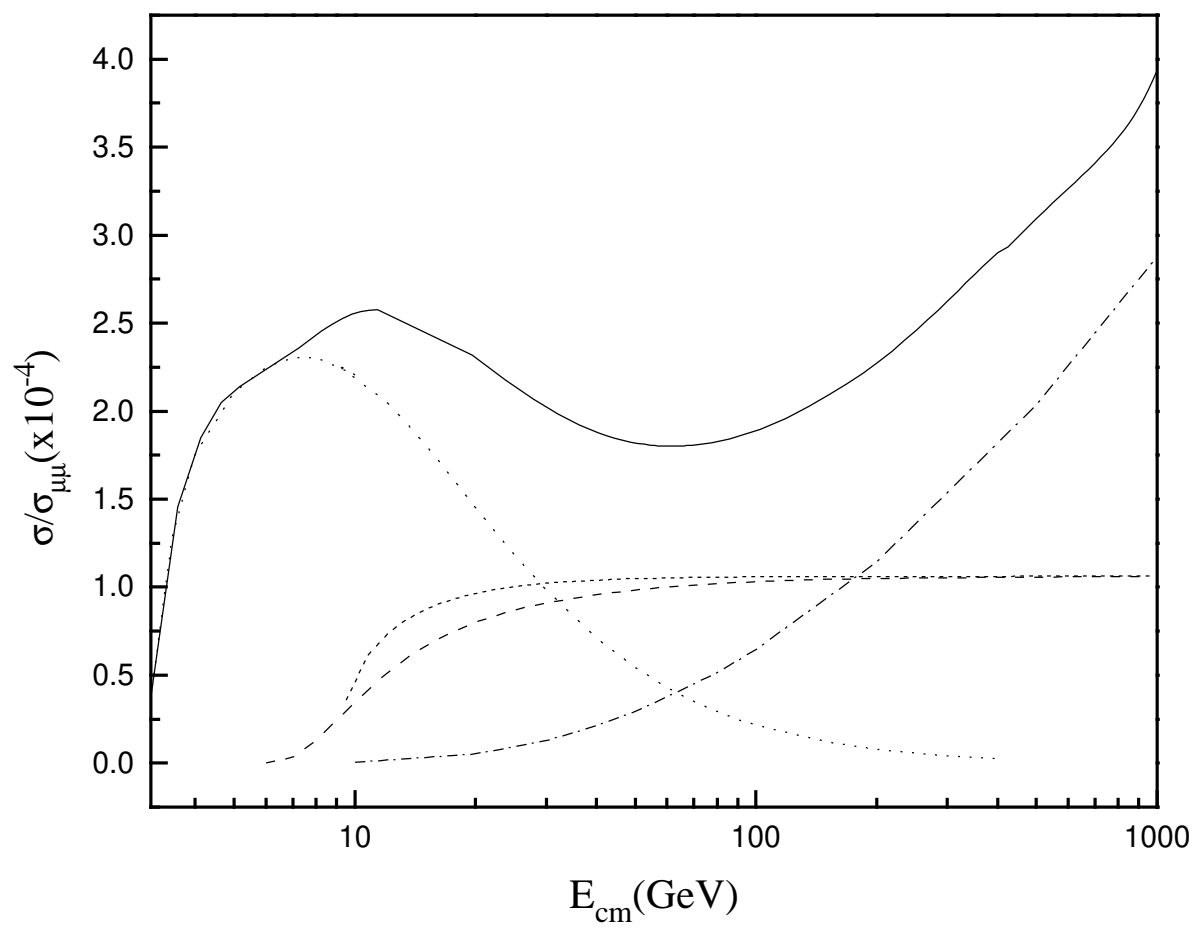


Fig.2



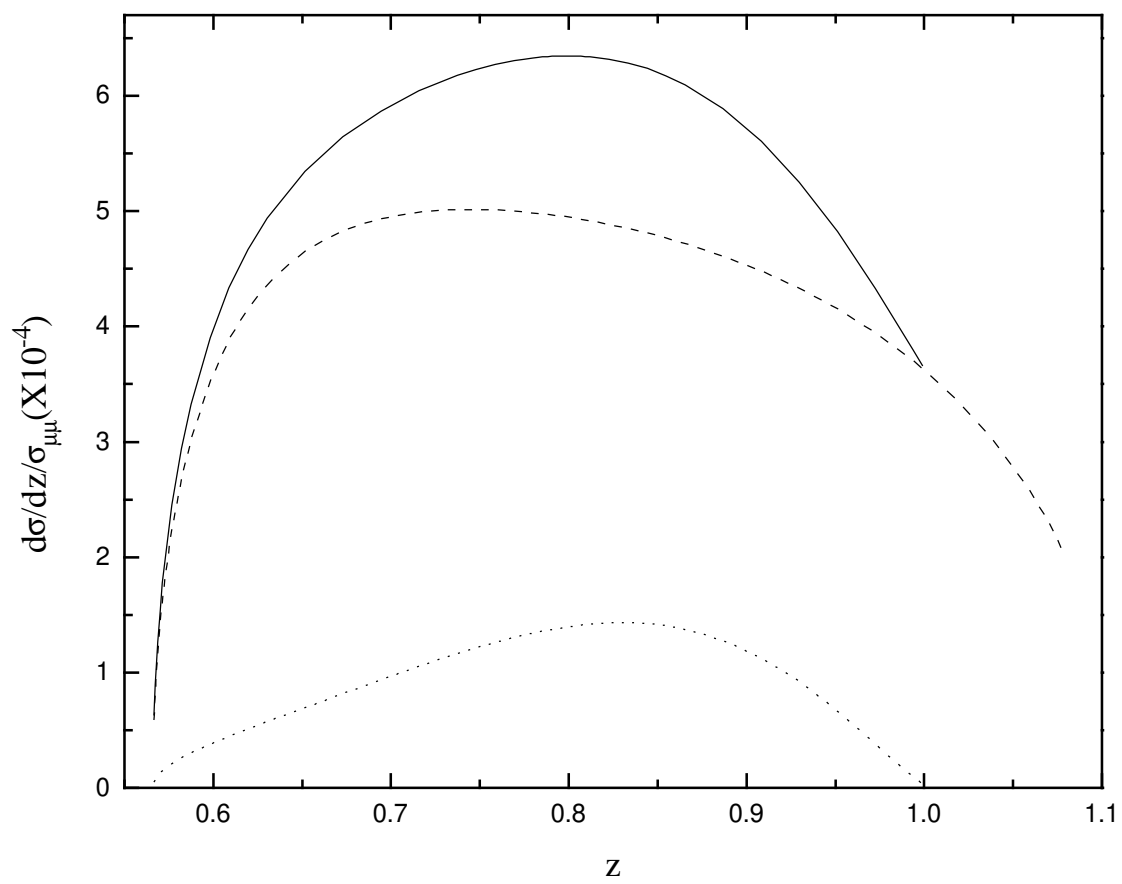


Fig.3(a)



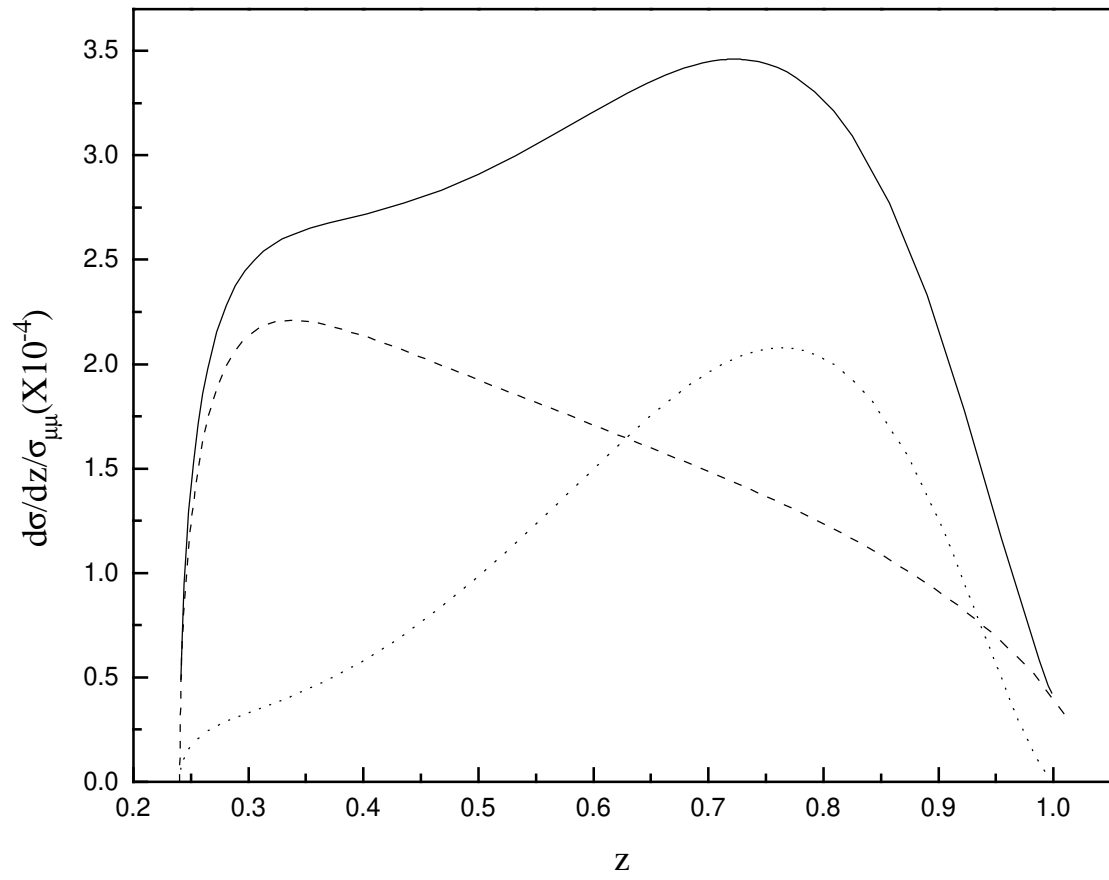


Fig.3(b)



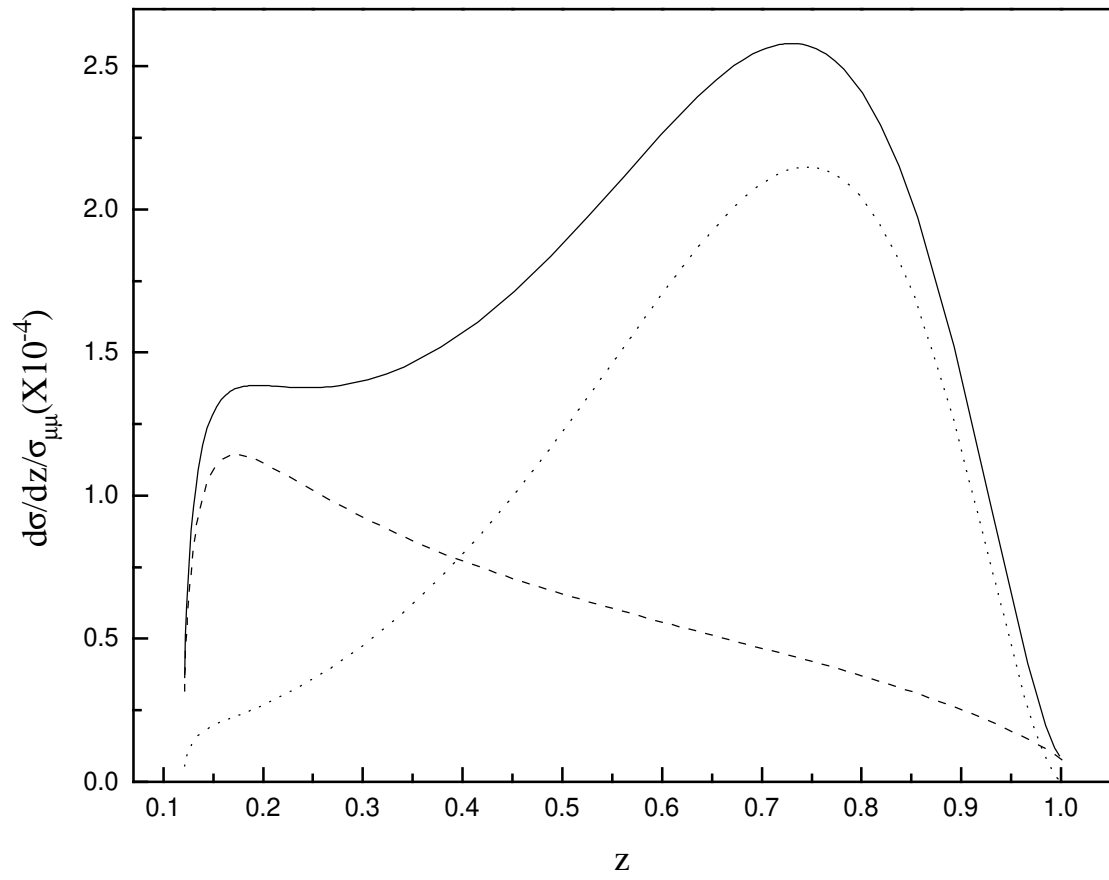


Fig.3(c)





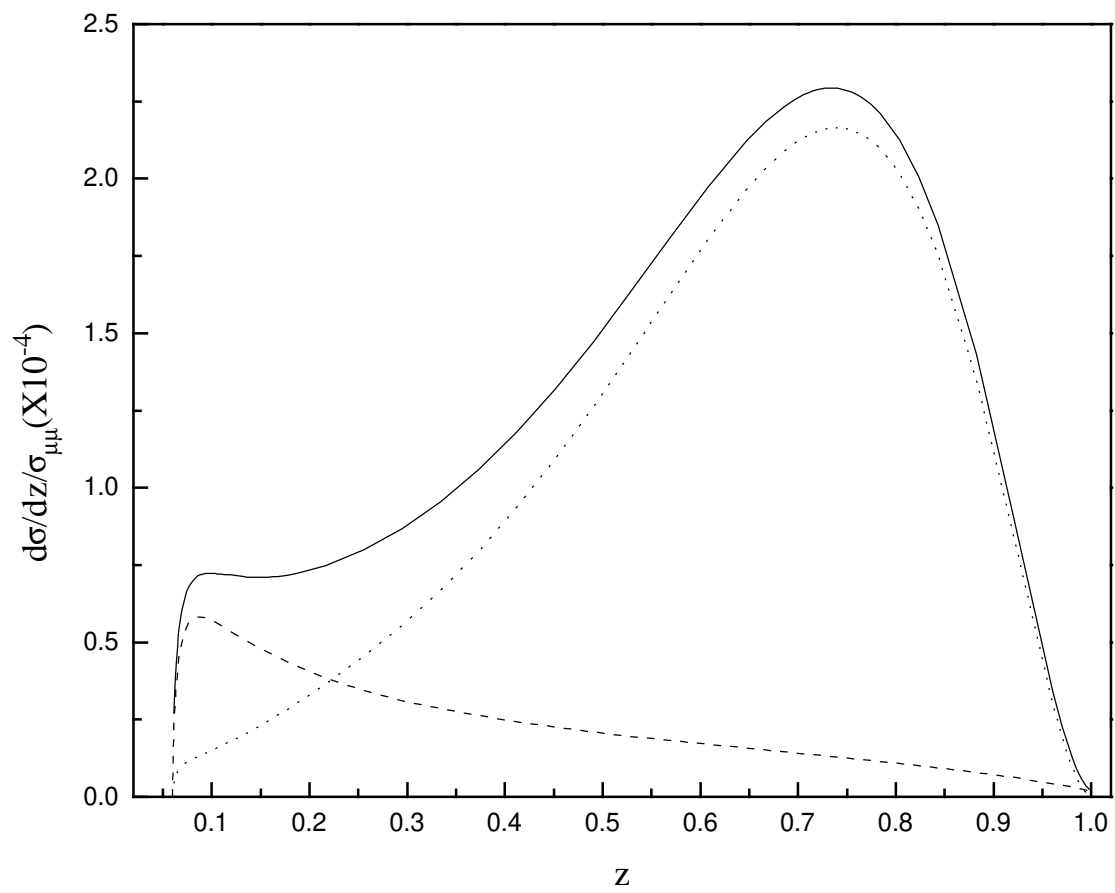
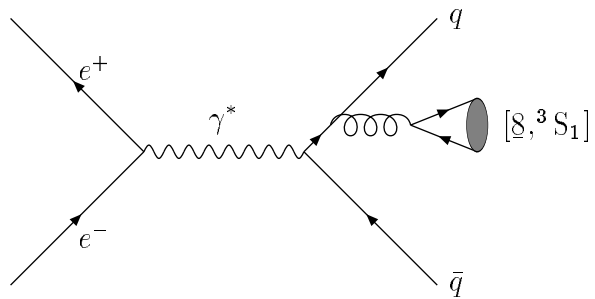
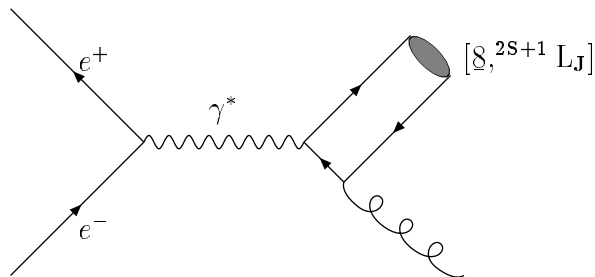


Fig.3(d)





(a)



(b)

Fig.4

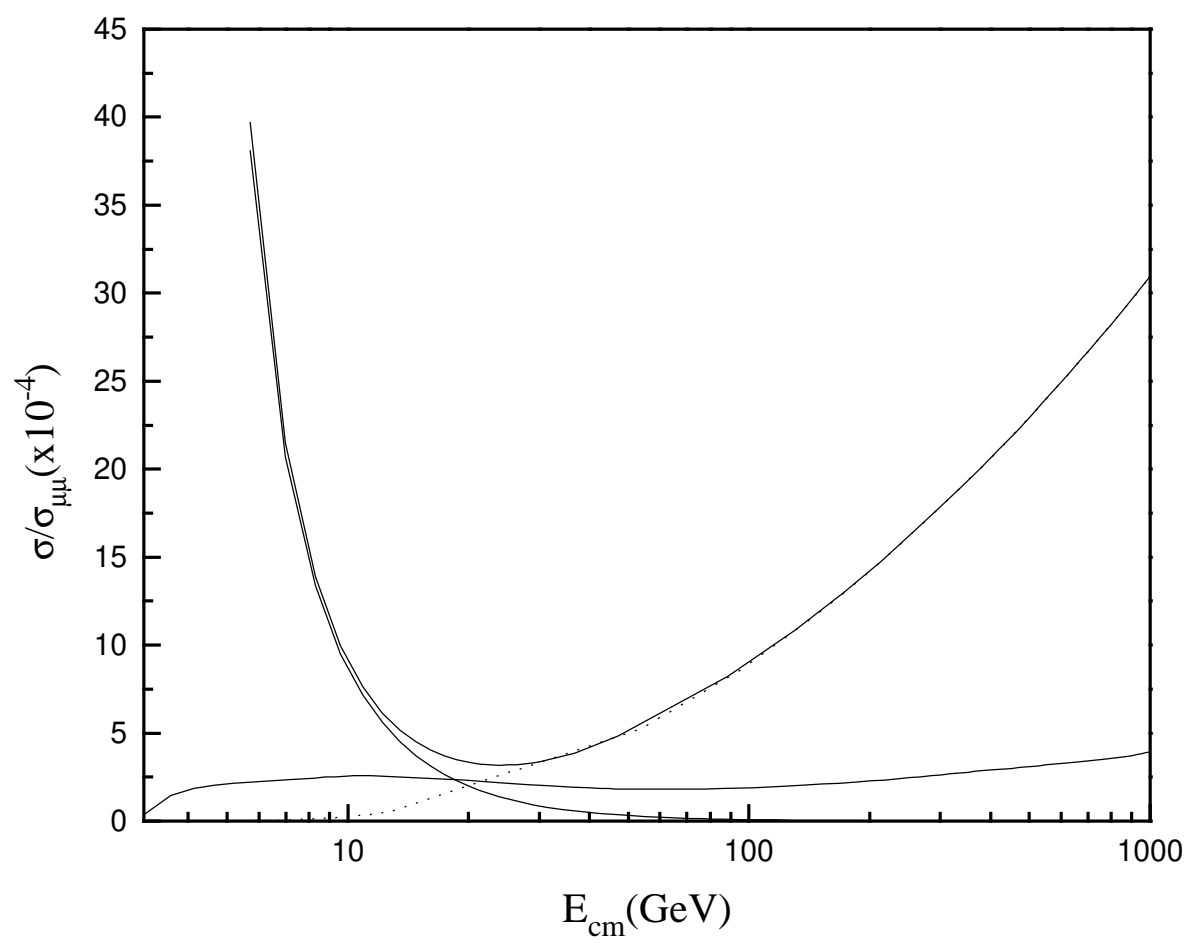


Fig.5



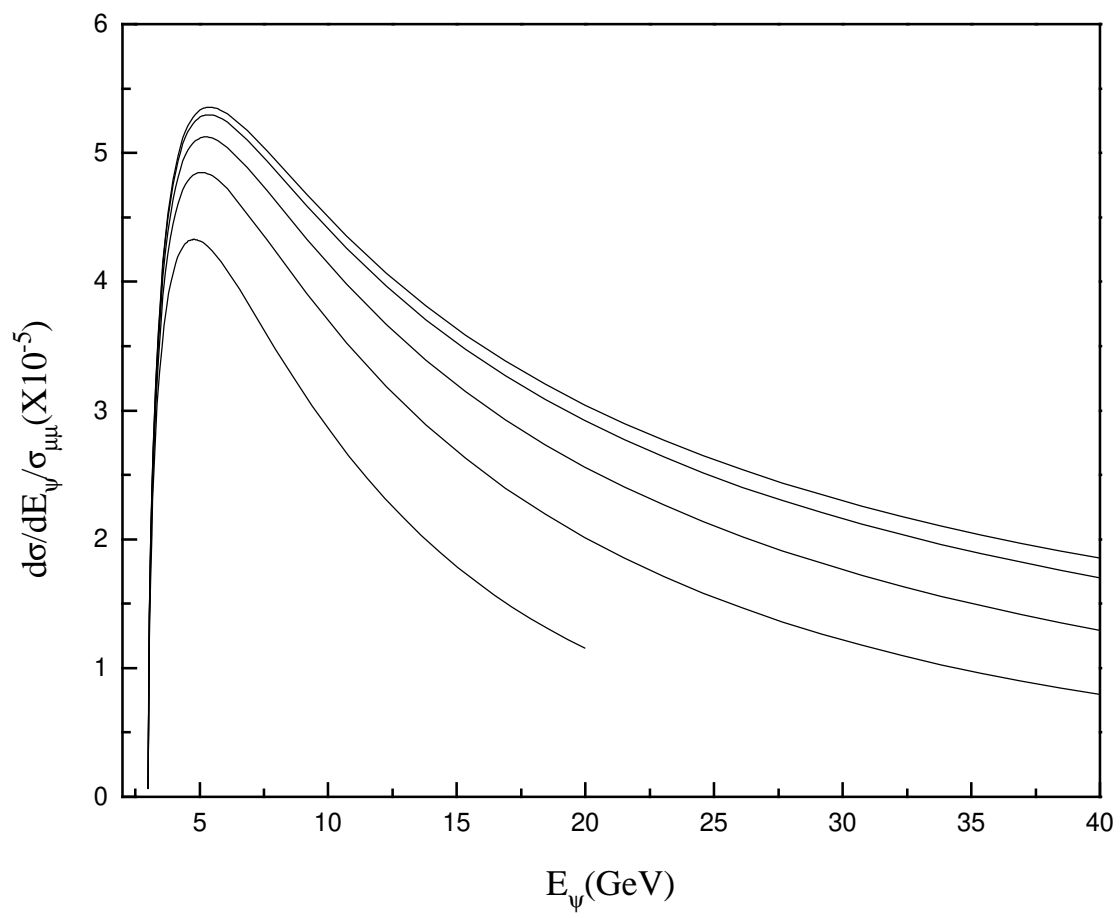


Fig.6

